Assessment of Load Characteristics in Short-Circuit Studies of Distribution Substations

Nguyen Thi Thanh Thuy*

Electrical Faculty, Thai Nguyen University of Technology, Thai Nguyen, Viet Nam

***Corresponding Author: thuyhtd@tnut.edu.vn**

DOI: https://dx.doi.org/10.51244/IJRSI.2025.1210000335

Received: 08 November 2025; Accepted: 15 November 2025; Published: 22 November 2025

ABSTRACT

This paper evaluates the influence of electrical loads on the distribution of currents under both normal and fault operating conditions in distribution substations. Static and dynamic loads are modeled using equivalent impedance components, where dynamic loads are represented by the Conventional Load Model, Exponential Load Model, Polynomial Load Model, and Comprehensive Load Model. The Newton-Raphson method is applied for power flow analysis to determine current distribution under normal operating states. In addition, the IEC short-circuit calculation method is adopted to analyze fault current distribution in the entire system under short-circuit conditions. A five-bus test system, in which the load can switch between static and composite (static + dynamic), is proposed to investigate current distribution under different operating conditions. Simulations are performed in ETAP for both normal and fault modes, considering static loads and composite loads. The results highlight current distribution across the system, clarifying the ability of dynamic loads to contribute to fault currents during short-circuit conditions, unlike static loads. The contributions of this study provide insights for designers and operators in understanding how electrical load characteristics affect the performance of protection devices in distribution substations.

Index Terms: Composed Load, Electrical Load Model, Static Load, Motor Load, Newton-Rahpson method, Short-Circuit Calculation.

INTRODUCTION

Electrical loads in distribution substations are diverse and vary depending on multiple factors, including technological advancements and consumption patterns. Each type of load possesses unique characteristics that influence the calculation of aggregated loads and the selection of protective devices. The contribution of loads to the current in different operating modes of the substation depends on both load types and operating states, and thus requires detailed evaluation.

Electrical loads in distribution substations are highly diverse and evolve in line with the development of production technologies as well as the consumption characteristics of different categories of equipment [1], [2]. Each type of load exhibits distinct characteristics that directly affect the calculation of aggregated loads and the selection of appropriate protective devices [3]. In power systems, loads are commonly categorized into Static Loads (SL) and Dynamic Loads (DL). Static loads include electrical equipment without rotating elements, such as lighting systems, electronic devices, and resistive appliances [4]. In contrast, dynamic loads are devices driven by electric motors, such as pumps, fans, or compressors, which, due to their mechanical inertia, can continue to supply energy for a short duration even after being disconnected from the power source [5], [6]. This characteristic allows dynamic loads to act as potential sources contributing to fault currents and thus must be taken into account in short-circuit analysis and protection system design [7]–[9].

In practical operation, loads in distribution substations often exist as Composed Loads (CL), i.e., a combination of static and dynamic loads. The proportion between these two components determines the electrical

ISSN No. 2321-2705 | DOI: 10.51244/IJRSI |Volume XII Issue X October 2025

characteristics at each bus, thereby affecting the selection of conductors, switching devices, and protection strategies [10], [11]. Recent studies have also indicated that the development of distributed generation and renewable energy sources has increased the demand for improved load models to more accurately reflect the operational behavior of modern distribution networks [12]–[14]. Furthermore, experimental results demonstrate the need to consider the ZIP characteristics (Z–Impedance, I–Current, P–Power) when modeling residential, commercial, and industrial loads [15].

Under normal operating conditions, loads determine the power and current levels that equipment must withstand over long durations, thereby influencing the lifetime and reliability of the system [16]. In fault conditions—particularly single-line-to-ground and three-phase short circuits—the current often far exceeds the rated value and may cause severe damage to conductive elements if not properly protected [2], [7]. Moreover, recent research shows that the participation of dynamic loads and renewable energy sources can significantly alter fault current distribution, necessitating adjustments in short-circuit analysis and relay protection design [8], [9], [12], [17], [18]. This is critical because the contribution of fault currents from dynamic loads can directly affect the breaking capability of circuit breakers, the operating conditions of relays, and the thermal endurance of conductors in distribution substations [13], [14], [19]–[21].

Based on the above analysis, this paper focuses on evaluating the impact of loads on current distribution in distribution substations. Section II presents the modeling methods of electrical loads, including static and dynamic loads. Section III introduces analytical methods for network operation under both normal and short-circuit conditions. Section IV presents simulation results, highlighting the differences between Static Loads (SL) and Composed Loads (CL). Finally, Section V concludes with key findings derived from this study.

LOAD MODELING

A. Static Load Model

A static load is defined by its active power (P), reactive power (Q), apparent power (S), and power factor (cosφ). The mathematical relationships of these parameters are expressed as follows [4]:

$$S = \sqrt{P^2 + Q^2} \qquad (1)$$

$$\cos\varphi = \frac{P}{S} \qquad (2)$$

where: P, Q, S are active power, reactive power, apparent power; cosφ is power factor.

Static loads typically consist of devices with constant or slowly varying currents, such as lighting equipment, electric heaters, or electronic devices. Their power consumption is nearly independent of sudden voltage changes, and thus, they rarely pose issues related to transient behavior or stability in the system.

B. Dynamic Load Models

Dynamic loads, particularly induction motors, represent the majority of industrial and commercial loads. Their operating characteristics differ significantly from static loads because they involve rotating mechanical components and inertia [5], [6]. When subject to voltage disturbances or during start-up, these loads exhibit non-linear behavior that strongly affects system stability. To analyze them accurately, different mathematical models are employed:

1) Conventional Load Model

The conventional representation assumes that the dynamic load can be modeled as a constant impedance at the fundamental frequency. This approach is widely applied in short-circuit studies because it allows motors to be represented as equivalent sources contributing to fault currents [4], [25].

ISSN No. 2321-2705 | DOI: 10.51244/IJRSI |Volume XII Issue X October 2025

Exponential Load Model [7-9], [25]:

$$P = P_0 \bar{U}^a \left(1 + K_{pf} \Delta f\right) \quad (3)$$

$$Q = Q_0 \bar{U}^b \left(1 + K_{qf} \Delta f\right) \quad (4)$$

where:

P_0, Q_0: reference active and reactive power at nominal voltage U_0;

P, Q are active power, reactive power at voltage U and frequency difference Δf;

$$\Delta f = \frac{f - f_0}{f_0};$$

f is current frequency of the system;

f_0 is norminal frequency of the system;

The parameters a and b represent the exponential indices that characterize the load behavior. Specifically, a value of 0 corresponds to a Constant Power load, a value of 1 corresponds to a Constant Current load, and a value of 2 corresponds to a Constant Impedance load. These indices are widely used in load modeling to capture the nonlinear dependence of power consumption on bus voltage;

K_{pf} =(0÷3) is the frequency-dependence coefficient of the active power component with respect to frequency deviation;

K_{qf} =(-2÷0) is the frequency-dependence coefficient of the reactive power component with respect to frequency deviation;

Polynomial Load Model [25]**:**

$$P = P_0 \left| p_1 \bar{U}^2 + p_2 \bar{U} + p_3 \right| \left(1 + K_{pf} \Delta f\right) \quad (5)$$

$$Q = Q_0 \left| q_1 \bar{U}^2 + q_2 \bar{U} + q_3 \right| \left(1 + K_{qf} \Delta f\right) \quad (6)$$

where: p_1, q_1, p_2, q_2, p_3, q_3 denote the power components corresponding to Constant Impedance, Constant Current, and Constant Power characteristics, respectively. Each portion of the load is defined by these constants.

Comprehensive Load Model:

The Comprehensive model of the Lumped Load uses the following equations to determine the real and reactive power components of the load [10], [11], [25]:

$$P = P_0 \left[P_{POLY} + P_{\text{EXP1}} + P_{\text{EXP2}} \right] \quad (7)$$

where:

$$P_{POLY} = p_1 \bar{U}^2 + p_2 \bar{U} + p_3$$

$$P_{\text{EXP1}} = p_4 \bar{U}^{a1} \left(1 + K_{pf1} \Delta f\right)$$

ISSN No. 2321-2705 | DOI: 10.51244/IJRSI |Volume XII Issue X October 2025

$$P_{EXP2} = p_5 \bar{U}^{a2} \left(1 + K_{pf2} \Delta f\right)$$

The formulation of the reactive load component follows an analogous structure, with reactive power compensation modeled explicitly. The comprehensive load model integrates both polynomial and exponential terms, parameterized by the constants p_1, q_1, p_2, q_2, p_3, q_3, p_4, q_4, p_5, q_5. These parameters describe the contributions of constant impedance, constant current, constant power, and exponential elements within the load.

The coefficients K_{pf1}, K_{pf2} correspond to the active power equations, typically varying in the range of 0 to 3.0. Similarly, the coefficients K_{qf1}, K_{qf2} pertain to the reactive power equations, with typical values ranging from –2.0 to 0.

In addition, short-circuit contribution levels are specified separately, in accordance with the IEC methodology, and are categorized as outlined in Table [2], [7], [25]

TABLE I. SHORT-CIRCUIT CONTRIBUTION

Short-Circuit Contribution	HP	Speed
High	Large	High RPM
Medium	Medium	Intermittent RPM
Low	Small	Low RPM

The lumped motor model includes parameters for grounding configuration, connection type, and rating. The grounding connection can be specified by selecting among the available options, with Wye and Delta being the supported types. The motor's short-circuit reactance-to-resistance ratio X_{sc}/R_a, commonly referred to as the X/R ratio, is also defined; if the *Typical* option is chosen, a standard representative value is automatically applied. In addition, the transient time constant T'_d, expressed in seconds, is considered, which is particularly relevant for calculations performed under the IEC 61363 methodology

$$T_d^{'} = \frac{X''}{2\pi f R_r} \qquad (8)$$

where: R_r is rotor resistance.

METHOD FOR POWER ANALYSIS UNDER NORMAL OPERATING CONDITIONS AND SHORT-CIRCUIT SCENARIOS

A. Power analysis under normal operating conditions

Mathematical model of medium voltage transmission lines is described in Fig. 1 [22-25].

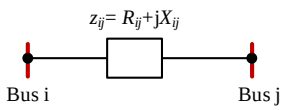

Fig. 1 Mathematical model of cable in low voltage systems

Where: R_{ij} (Ω) is resistance and X_{ij} (Ω) is reactance of the transmission line connecting bus i and bus j.

Mathematical model of two-winding transformer is described in Fig. 2.

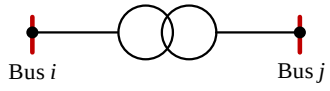

a. Power transformer

ISSN No. 2321-2705 | DOI: 10.51244/IJRSI |Volume XII Issue X October 2025

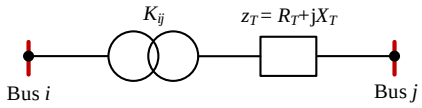

b. Equivalent circuit

Fig. 2 Mathematical model of two-winding transformer

Where: R_T (Ω) is resistance and X_T (Ω) is reactance of the transformer; K_{ij} is voltage ratio between bus i and bus j of ideal transformer (without power loss). In Fig. 2b, voltage value of bus i is higher than voltage value of bus j, so bus i is called HV bus and bus j is called LV bus.

A general distribution system include (N+1) buses, where N buses are normal buses and a bus is ground. Any branch in the system can be classified to the standard line or transformer branch. These branches can be defined by a general standard branch as depicted in Fig. 3 [22-25].

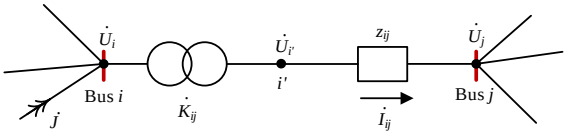

a. Bus *i* connecting to the ideal transformer directly

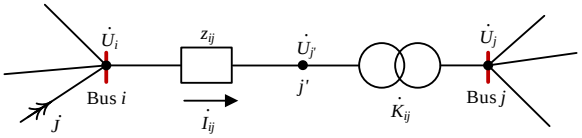

b. Bus i connecting to the ideal transformer indirectly through an impedance

Fig. 3 Diagram of general standard branch

In Fig. 3a and Fig. 3b, the current source $\dot{J}_i$ (from generations) is injects to bus i. If the branch describes a transformer, voltage ratio can be calculated forward to bus i that is $\dot{K}_{ij} = \frac{\dot{U}_{i'}}{\dot{U}_{i}}$. If the branch describes a transmission line, voltage ratio is $\dot{K}_{ij} = 1$.

Applying Kirchhoff 1, current balancing equation at bus i can be determined by (9) [7].:

$$\sum_{\substack{j=0 \\ j\neq i}}^{N} \dot{I}_{ij} = \dot{J}_i \qquad (9)$$

Using I'_{ij}, equation (1) can be converted to equation (10):

$$\sum_{\substack{j=0 \\ j\neq i}}^{N} \dot{K}_{ij}\dot{I}'_{ij} = \dot{J}_i \qquad (10)$$

Using Ohm's law for *i'j* branch, equation (3) can be converted to equation (11) [7]:

$$\dot{Y}_{ii}\dot{U}_k + \sum_{\substack{j=0 \\ j\neq i}}^{N} \dot{Y}_{ij}\dot{U}_j = \dot{J}_i \qquad (11)$$

where: $\dot{Y}_{ii}$ is individual admittance of bus i and $\dot{Y}_{ij}$ is interactive admittance of branch ij.

ISSN No. 2321-2705 | DOI: 10.51244/IJRSI |Volume XII Issue X October 2025

$\dot{Y}_{ii}$, $\dot{Y}_{ij}$ can be determined by equation (12) and (13):

$$\dot{Y}_{ii} = \sum_{\substack{j=0 \\ j\neq i}}^{N} \left(\frac{\dot{K}_{ij}^2}{\dot{Z}_{ij}} \right) \quad (12)$$

$$\dot{Y}_{ij} = -\frac{\dot{K}_{ij}}{\dot{Z}_{ij}} \quad (13)$$

Working the same with Fig. 7b, $\dot{Y}_{ii}$ can be defined by equation (14):

$$\dot{Y}_{ii} = \sum_{\substack{j=0 \\ j\neq i}}^{N} \frac{1}{\dot{Z}_{ij}} \quad (14)$$

In general case study, bus *i* can be connected to *m* buses directly through ideal transformers and *k* buses indirectly through ideal transformers. $\dot{Y}_{ii}$ can be determined by equation (15) [22-25]:

$$\dot{Y}_{ii} = \sum_{\substack{j=0 \\ j\neq i}}^{k} \frac{1}{\dot{Z}_{ij}} + \sum_{\substack{j=0 \\ j\neq i}}^{m} \frac{\dot{K}_{ij}^2}{\dot{Z}_{ij}} \quad (15)$$

Current balancing equations for whole system can be described in system of equations (16).

$$\begin{cases} \dot{Y}_{11}\dot{U}_1 + \dot{Y}_{12}\dot{U}_2 + ... + \dot{Y}_{1N}\dot{U}_N = \dot{J}_1 \\ \dot{Y}_{21}\dot{U}_1 + \dot{Y}_{22}\dot{U}_2 + ... + \dot{Y}_{2N}\dot{U}_N = \dot{J}_2 \\ ..... \\ \dot{Y}_{N1}\dot{U}_1 + \dot{Y}_{N2}\dot{U}_2 + ... + \dot{Y}_{NN}\dot{U}_N = \dot{J}_N \end{cases} \quad (16)$$

From system of equations (16), matrix admittance can be derived as (17):

$$Y = \begin{bmatrix} \dot{Y}_{11} & \dot{Y}_{12} & ... & \dot{Y}_{1N} \\ \dot{Y}_{21} & \dot{Y}_{22} & ... & \dot{Y}_{2N} \\ ... & ... & ... & ... \\ \dot{Y}_{N1} & \dot{Y}_{N2} & ... & \dot{Y}_{NN} \end{bmatrix} \quad (17)$$

Almost buses in distribution systems are PQ buses (load buses). Capacitors can be implemented at these buses and considered as reactive generators. In these systems, Newton-Raphson method is often used to determine power flows and voltage buses.

To determine operating parameters for *N*-bus grid by using Newton-Raphson method, system of power balancing equations at bus i can be defined by (18) and (19) [7]:

$$U_i^2 y_{ii} \cos\psi_{ii} + \sum_{\substack{j=1 \\ j\neq i}}^{N} U_i U_j y_{ij} \cos(\delta_i - \delta_j - \psi_{ij}) - P_{Li} = \Delta P_i \quad (□8)$$

$$-U_i^2 y_{ii} \sin\psi_{ii} + \sum_{\substack{j=1 \\ j\neq i}}^{N} U_i U_i y_{ij} \sin(\delta_i - \delta_j - \psi_{ij}) - (Q_{Li} - Q_{Ci}) = \Delta Q_i \quad (□9)$$

where: $i = \overline{1,N}; \dot{U}_i = U_i \angle \delta_i; Y_{ij} = y_{ij} \angle \Psi_{ij}$.

ISSN No. 2321-2705 | DOI: 10.51244/IJRSI |Volume XII Issue X October 2025

P_{Li} and Q_{Li} are active and reactive load power at the bus i; Q_{Ci} are active and reactive power of the capacitor bank at the bus i.

From solutions at the k[th] step including $\delta_i^{(k)}$ and $U_i^{(k)}$, values of $\Delta P_i^{(k)}$ and $\Delta Q_i^{(k)}$ can be calculated. Moreover, values of $\Delta\delta_i^{(k)}$ and $\Delta U_i^{(k)}$ at the k[th] step can be calculated by using reversed Jacobian matrix as described in equation (20):

$$\begin{bmatrix} \Delta\delta_i^{(k)} \\ \Delta U_i^{(k)} \end{bmatrix} = J^{-1} \begin{bmatrix} \Delta P_i^{(k)} \\ \Delta Q_i^{(k)} \end{bmatrix} \qquad (20)$$

where: J is Jacobian matrix.

Jacobian matrix at the i^{th} step: $J = \begin{bmatrix} J_1 & J_2 \\ J_3 & J_4 \end{bmatrix}$

Solutions at the next step can be determined by equation (14) [20-21]:

$$\begin{bmatrix} \delta_i^{(k+1)} \\ U_i^{(k+1)} \end{bmatrix} = \begin{bmatrix} \delta_i^{(k)} \\ U_i^{(k)} \end{bmatrix} + \begin{bmatrix} \Delta\delta_i^{(k)} \\ \Delta U_i^{(k)} \end{bmatrix} \qquad (21)$$

This process will be stopped if both values of ΔP_i and ΔQ_i are smaller than allowable value ε [7-9]. Fig. 4 describes the Newton-Raphson method to analyze a distribution system.

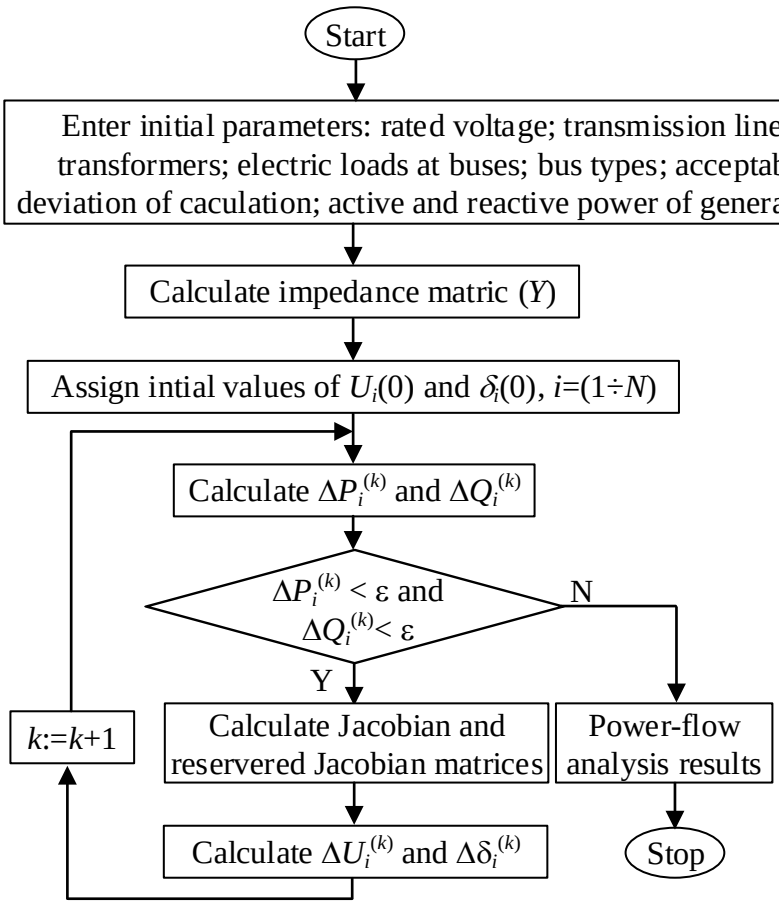

Fig. 4. Newton-Raphson algorithm to analyze whole grid

The Newton–Raphson method is characterized by quadratic convergence, enabling significantly faster convergence compared to alternative load flow techniques. Its convergence process is guided by well-defined

criteria that control the permissible mismatches in real and reactive power at each bus, thereby allowing direct specification of the desired solution accuracy. In practical applications, the convergence tolerance is typically set to 0.001 MW for active power and 0.001 MVAr for reactive power.

Despite its efficiency, the method is sensitive to the choice of initial bus voltage values. To enhance numerical stability and reliability, careful initialization is recommended. In ETAP, several Gauss–Seidel iterations are performed prior to executing the Newton–Raphson load flow, ensuring a consistent and well-conditioned set of initial bus voltages.

B. Method for power analysis under fault conditions in accordance with IEC standard

IEC 60909 and related standards categorize short-circuit currents based on their magnitudes (maximum and minimum) as well as their distance from the generator (near and far). Maximum short-circuit currents are used to determine equipment rating requirements, while minimum short-circuit currents are critical for setting protective devices. The classification into near-to-generator and far-from-generator faults dictates whether the decay of the AC component should be explicitly considered in the calculation.

The three-phase short-circuit current (I''_k) is evaluated using the following expression [22–25]:

$$I_k^{"} = \frac{cU_n}{\sqrt{3}Z_{(1)}} \qquad (22)$$

Two-phase short-circuit current (I''_{k2}) is calculated using the following formula:

$$I_{k2}^{"} = \frac{cU_n}{\left|\dot{Z}_{(1)} + \dot{Z}_{(2)}\right|} = \frac{cU_n}{2\left|\dot{Z}_{(1)}\right|} = \frac{\sqrt{3}}{2} I_k^{"} \qquad (23)$$

Two-phase-to-ground short-circuit current (I''_{kE2E}) is calculated using the following formula [22-25]:

$$I''_{kE\,2E} = \frac{\sqrt{3}cU_{dm}}{\left|\dot{Z}_{(1)} + 2\dot{Z}_{(0)}\right|} \qquad (24)$$

Single-phase-to-ground short-circuit current (I''_{k1}) is calculated using the following formula [22-25]:

$$I_{k1}^{"} = \frac{\sqrt{3}cU_n}{\left|2\dot{Z}_{(1)} + \dot{Z}_{(0)}\right|} \qquad (25)$$

where: Z_k is the equivalent impedance at the fault location; U_n is the normial grid voltage; $Z_{(1)}$, $Z_{(2)}$ và $Z_{(0)}$ are the positive-sequence, negative-sequence, and zero-sequence impedances, respectively, from the source to the fault location.

Voltage factor *c*: This is the factor used to adjust the value of the equivalent voltage source for minimum and maximum current calculations according to the following table.

TABLE II. VOLTAGE FACTOR (±5% VOLTAGE TOLERANCE)

Nominal Voltage U_n	For Maximum Short-Circuit Current Calculation (c_{max})	For Minimum Short-Circuit Calculation (c_{min})
Others < 1000 V	1.05	0.95
Medium voltage: > 1 kV to 230 kV	1.10	1.00
High voltage: > 230 kV	1.10	1.00

ISSN No. 2321-2705 | DOI: 10.51244/IJRSI |Volume XII Issue X October 2025

TABLE III. VOLTAGE FACTOR (±10% VOLTAGE TOLERANCE)

Nominal Voltage U_n	For Maximum Short-Circuit Current Calculation (c_{max})	For Minimum Short-Circuit Calculation (c_{min})
Others < 1000 V	1.10	0.90
Medium voltage: > 1 kV to 230 kV	1.10	1.00
High voltage: > 230 kV	1.10	1.00

SIMULATION

A. Simulation parameters

Consider the power system network of a distribution substation with five buses, as illustrated in Fig. 5, hereafter referred to as the E-5bus system.

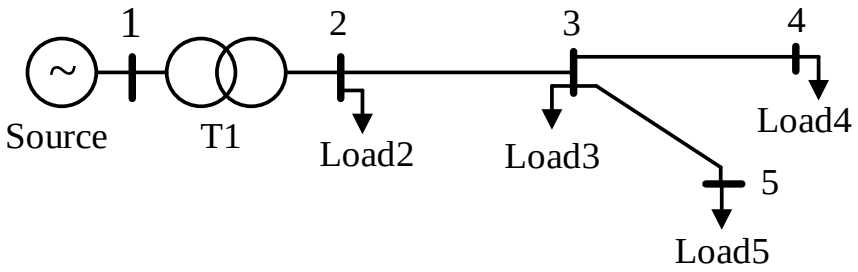

Fig. 5. Diagram of E-5bus

Parameters of transmission lines in Table IV, power source in Table V, transformers in Table VI, electric load at bused using exponential model in Table VII.

TABLE IV. PARAMETERS OF TRANSMISSION LINES

Name	Sectional area of a conductor (mm^2)	Insulation	Length (m)	Number of conductors/phase
Bus B2 - Bus B3	400	XLPE	100	1
Bus B3 - Bus B4	240	XLPE	60	1
Bus B3 - Bus B5	95	XLPE	50	1

TABLE V. PARAMETERS OF SOURCE

Type	Parameters
Power system	Rated voltage: 22 kV; Short-circuit power: 300 MVA; Reactance/Resistance: 10

TABLE VI. TRANSFORMERS

Location	Parameters
T1	Voltage ratio: 22/0.4 kV; Rated power: 4 MVA; Impedance: Z=8.35%; Reactance/Resistance=13

TABLE VII. PARAMETERS OF ELECTRIC LOAD AT BUSES

Name	Static load and conventional load			Composed load (Exponential model)					
	Power (kVA)	Power factor	Ratio	P_0 (kW)	Q_0 (kVAr)	a	b	K_{pf}	K_{qf}
Load B2	250	0.9	50%	230	100	1	2	0.1	0.1
Load B3	180	0.9	50%	162	80	2	1	0.1	0.1
Load B4	400	0.9	50%	230	100	1	1	0.2	0.2
Load B5	250	0.9	50%	360	175	3	1	0.15	0.1

ISSN No. 2321-2705 | DOI: 10.51244/IJRSI |Volume XII Issue X October 2025

B. Simulation results

The Newton–Raphson method and ETAP software are employed to simulate the E-5bus network using the parameters provided in the above table. The simulation results for the operating condition with all static loads are presented in Fig. 6, while the aggregated load modeled with the conventional approach is illustrated in Fig. 7. The results of three-phase and single-phase short-circuit faults at location F1 are shown in Fig. 8 for the static load case and in Fig. 9 for the dynamic load case.

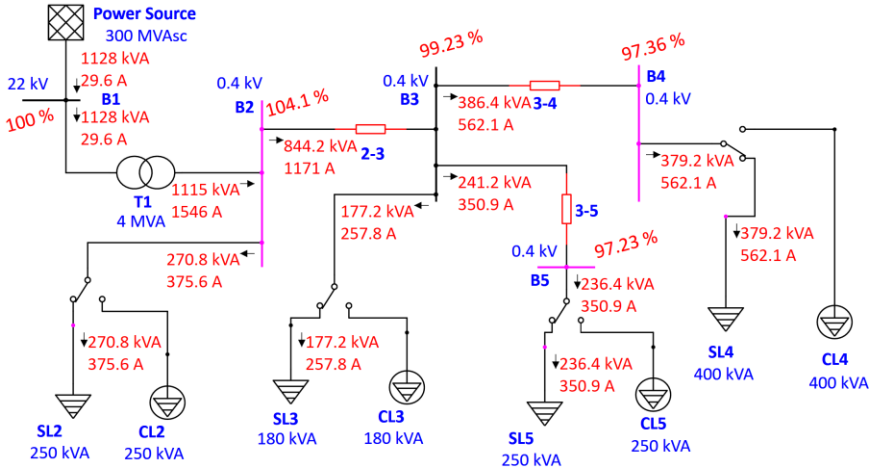

Fig. 6 Current distribution under normal operating conditions when all loads are static, based on the Conventional Model

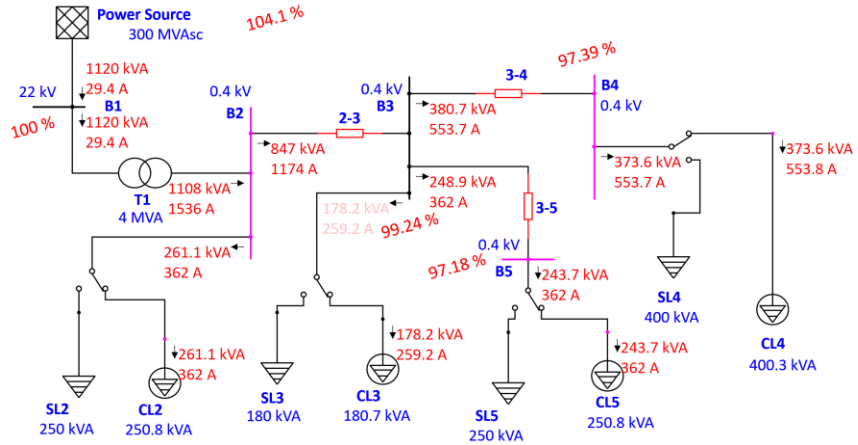

Fig. 7 Current distribution under normal operating conditions with mixed loads, based on the Conventional Model

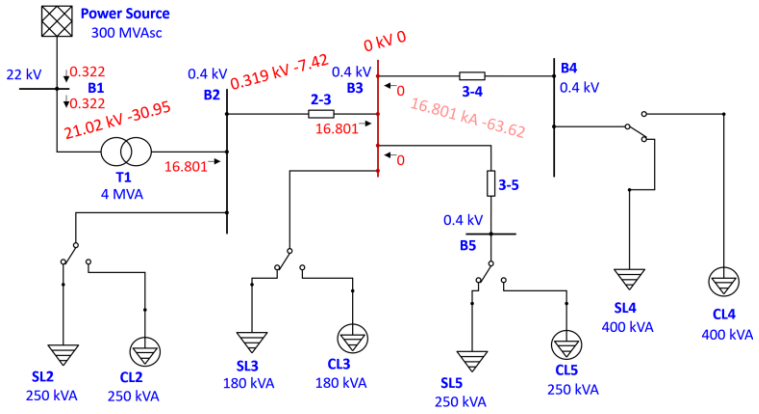

a. Three-phase short circuit

ISSN No. 2321-2705 | DOI: 10.51244/IJRSI |Volume XII Issue X October 2025

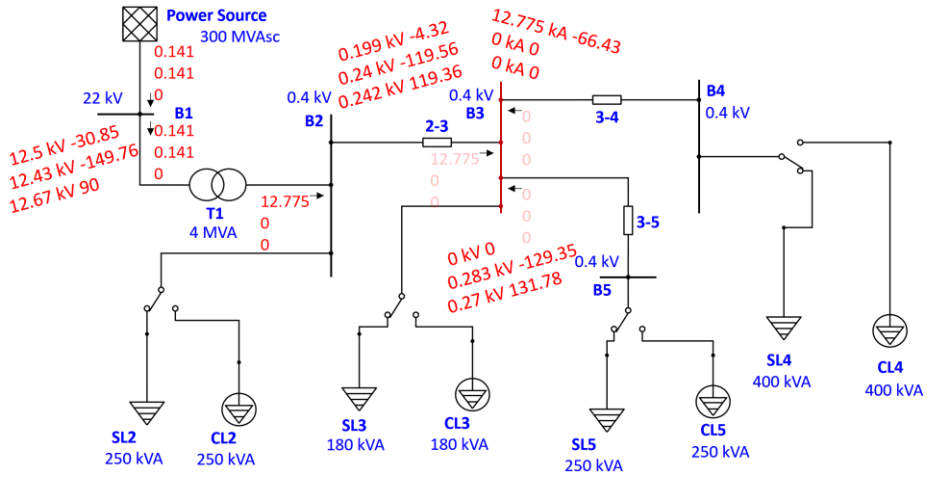

b. Single-phase-to-ground short circuit

Fig. 8 Current distribution under fault condition at bus B3 when all loads are static, based on the Conventional Model.

The simulation results of three-phase and single-phase short-circuit faults at fault location F1 are presented in Fig. 9.

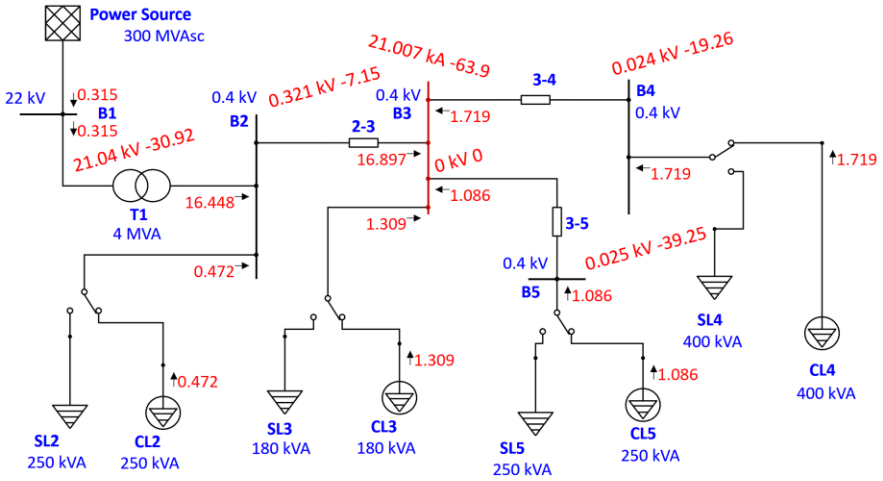

a. Three-phase short circuit

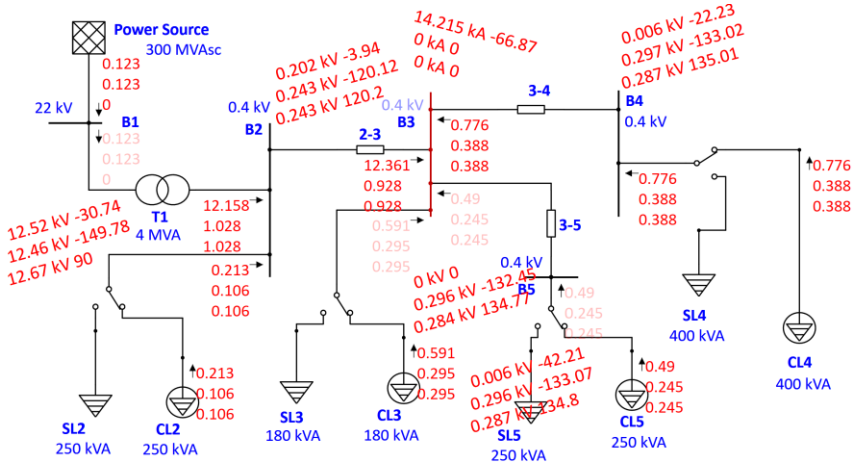

b. Single-phase-to-ground short circuit

Fig. 9 Current distribution under fault condition at bus B3 with mixed loads, based on the Conventional Model

ISSN No. 2321-2705 | DOI: 10.51244/IJRSI |Volume XII Issue X October 2025

The simulation results of three-phase and single-phase short-circuit faults at fault location F2 are shown in Fig. 10 for static loads and Fig. 11 for dynamic loads.

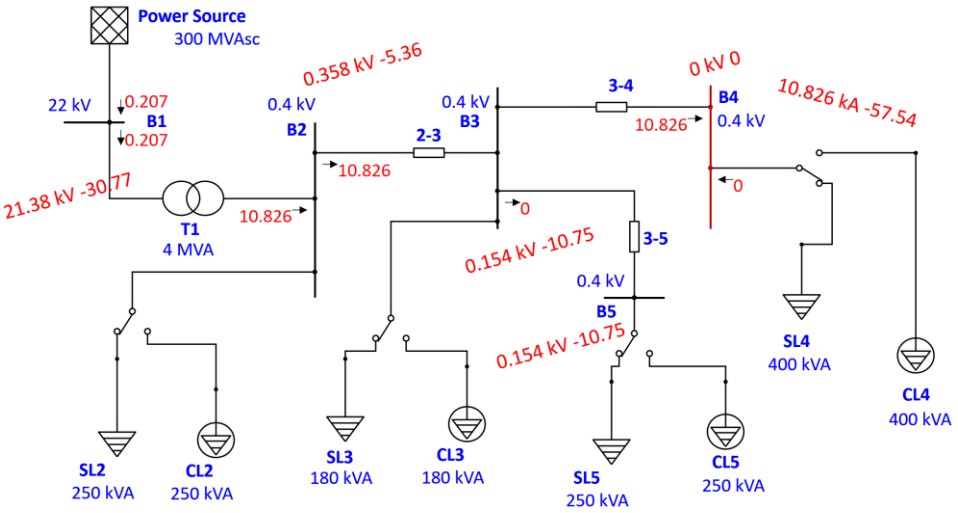

a. Three-phase short circuit

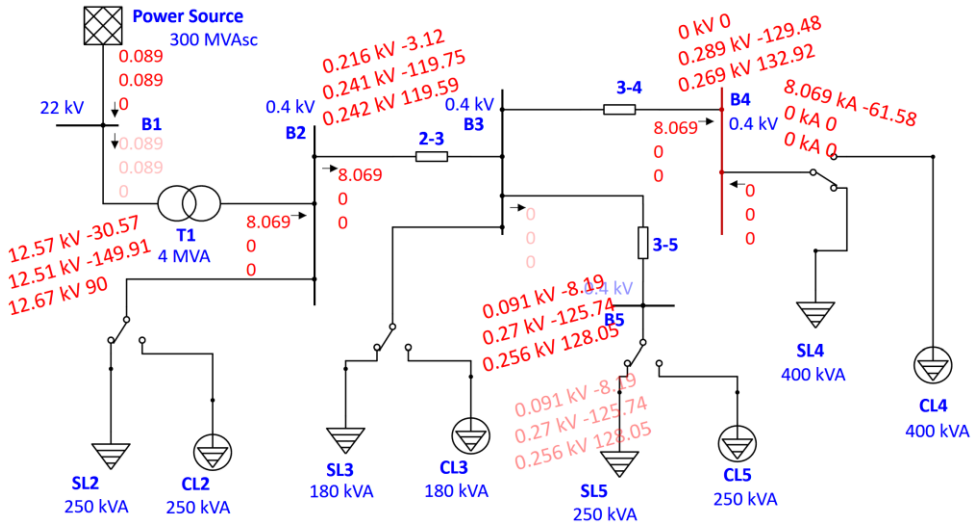

b. Single-phase-to-ground short circuit

Fig. 10 Current distribution under fault condition at bus B4 when all loads are static, based on the Conventional Model

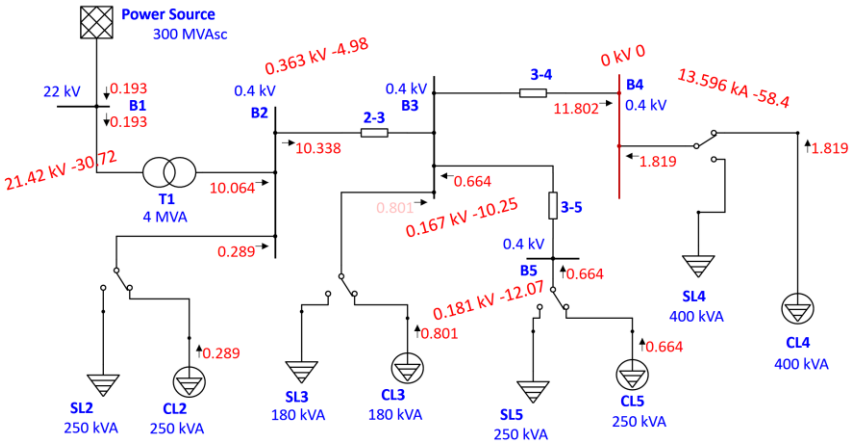

a. Three-phase short circuit

ISSN No. 2321-2705 | DOI: 10.51244/IJRSI |Volume XII Issue X October 2025

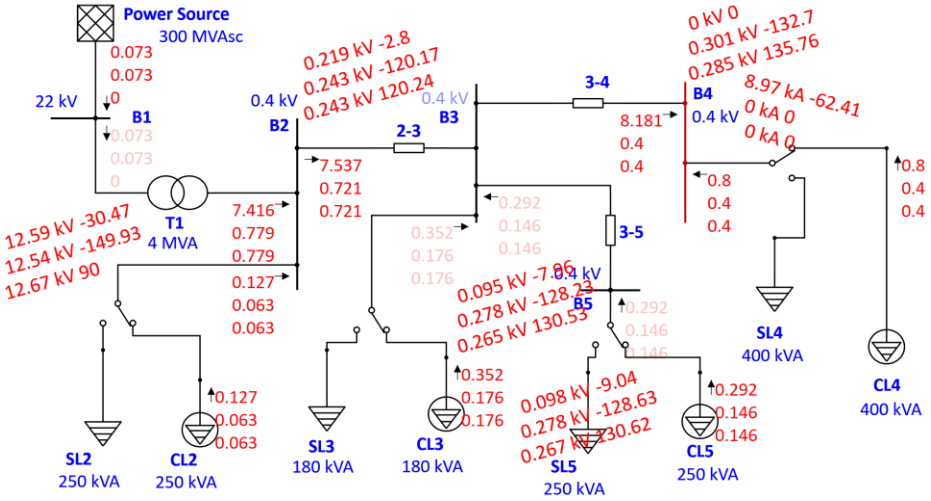

b. Single-phase-to-ground short circuit

Fig. 11 Current distribution under fault condition at bus B4 with mixed loads, based on the Conventional Model

From the above simulation results, the current distribution across the entire network under normal operating conditions, for both static and aggregated loads, is illustrated in Fig. 12.

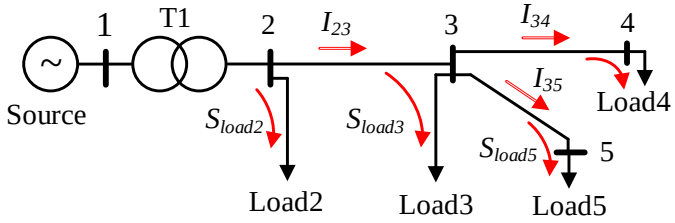

Fig. 12 Current distribution under normal operating conditions, based on the Conventional Model

For a short-circuit fault at F1, the current distribution in the network is shown in Fig. 13a for static loads and in Fig. 13b for aggregated loads.

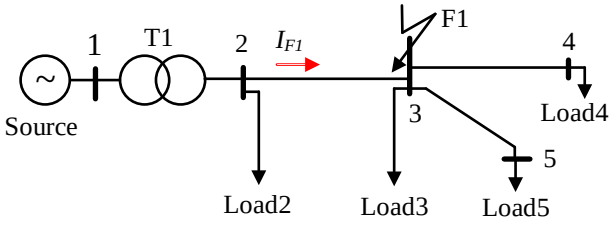

a. Loads including all static components

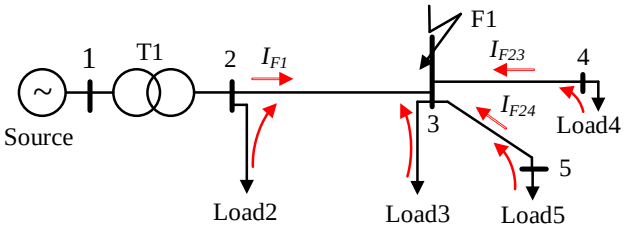

b. Load including dynamic components

Fig. 13 Current distribution in the substation under a fault at F1, based on the Conventional Model

ISSN No. 2321-2705 | DOI: 10.51244/IJRSI |Volume XII Issue X October 2025

For a short-circuit fault at F2, the current distribution in the network is shown in Fig. 14a for static loads and in Fig. 14b for aggregated loads.

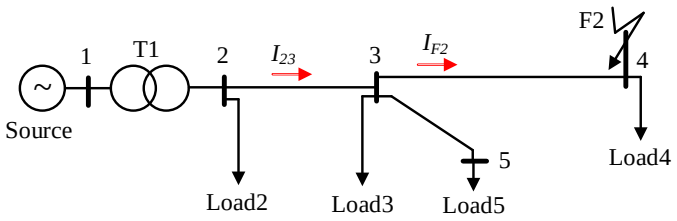

a. Loads including all static components

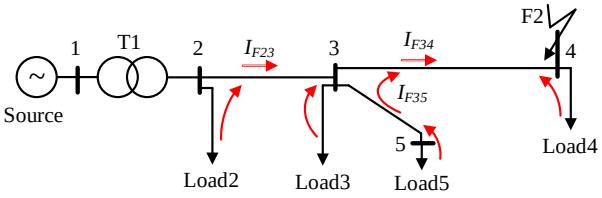

b. Load including dynamic components

Fig. 14 Current distribution in the substation under a fault at F2, based on the Conventional Model

The simulation results of current distribution considering the Exponential Load Model under a short-circuit fault at F1 are illustrated in Fig. 15.

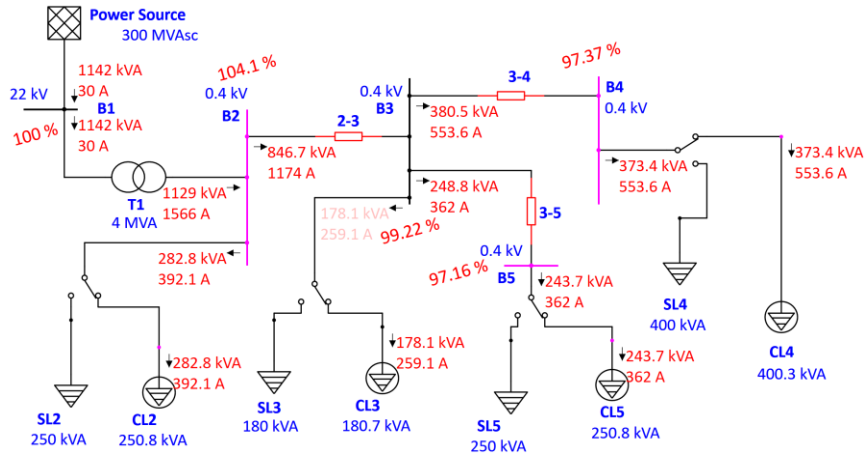

a. Normal operating conditions

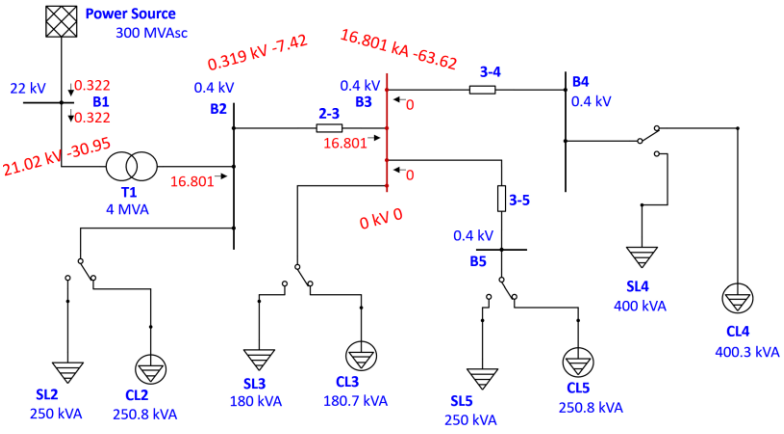

b. Three-phase short circuit

ISSN No. 2321-2705 | DOI: 10.51244/IJRSI |Volume XII Issue X October 2025

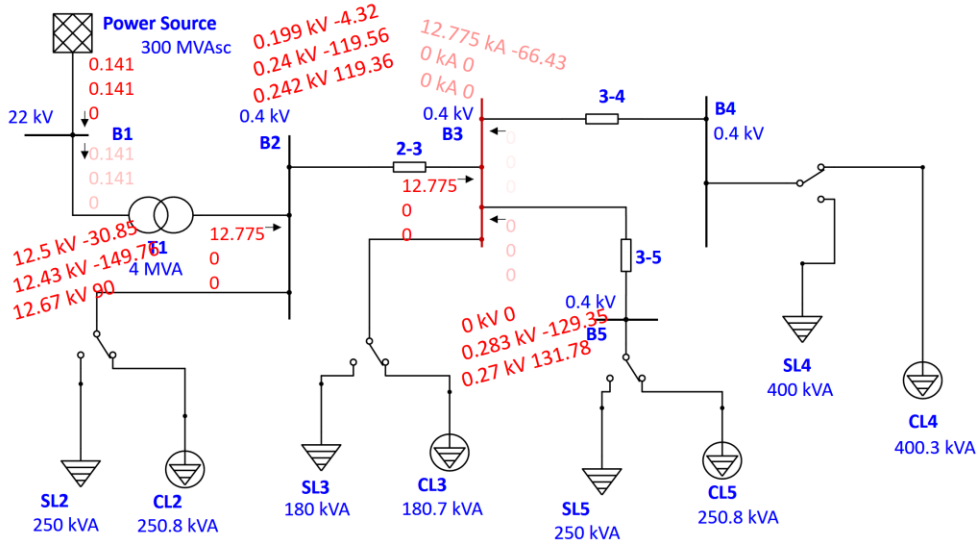

c. Single-phase-to-ground short circuit

Fig. 5 Current distribution in the substation under a fault at F1 based on the Exponential Load Model

The above figures demonstrate that the overall current distribution in the network remains unchanged regardless of whether the load is static or dynamic. In the case of static loads under fault conditions, the load does not contribute any current to the fault location, irrespective of the fault position within the network. By contrast, when dynamic loads are considered under the Conventional Model, the loads contribute current to the fault location, regardless of whether the fault occurs at the sending or receiving end of the feeder. The magnitude of the fault current contribution depends on the proportion of motor load: the larger the motor share, the greater the contribution. Under fault conditions with motor participation, the motors behave as internal sources, injecting fault current into the fault point. However, under the Exponential Load Model, dynamic loads do not contribute any current to the fault location, and the other load models yield similar results.

CONCLUSIONS

The contribution of this paper is the assessment of the impact of static and dynamic loads on the distribution of short-circuit currents in distribution substations. These load types are modeled through various approaches, including the Static Load Model, Conventional Load Model, Exponential Load Model, Polynomial Load Model, and Comprehensive Load Model. The Newton–Raphson method is applied for load flow analysis under normal operating conditions, while the IEC short-circuit calculation methodology is employed to determine operating parameters under fault conditions. All system components are modeled and analyzed in ETAP software.

The simulation results indicate that the current distribution and bus voltage parameters under normal operating conditions are not affected by the type of load. This implies that the steady-state operation of the substation, which corresponds to its long-term performance, remains independent of load characteristics. Under fault conditions, however, motor loads influence fault current contributions when represented by the Conventional Load Model, in which the load behaves as an additional current source at the fault location. In contrast, when the Exponential, Polynomial, or Comprehensive Load Models are used, the load does not contribute to fault current under any fault scenario. In such cases, dynamic loads behave equivalently to static loads with respect to short-circuit current contribution.

The findings of this study can be applied to the design and operation of distribution substations. Designers and operators must carefully select appropriate load models and account for the extent of load contribution to short-circuit currents in order to properly coordinate protection systems and evaluate fault current magnitudes. Future work will further investigate the design and operation of protective relaying systems, explicitly considering the contribution of load current during fault conditions.

ACKNOWLEDGMENTS

This study is completely supported by Thai Nguyen University of Technology, Thai Nguyen University, Viet Nam.

REFERENCES

1. S. Subedi, H. Zhou, H. Karki, and B. Poudel, "Aggregate data-driven dynamic modeling of active distribution networks with DERs for voltage stability studies," *IET Renewable Power Generation*, vol. 18, no. 6, pp. 678–689, Jun. 2024.
2. Y. Liu, Z. Guo, and X. Zhang, "Real-time short-circuit current calculation in electrical distribution systems considering the uncertainty of renewable resources and electricity loads," *Applied Sciences*, vol. 14, no. 23, p. 11001, 2024.
3. S. Hill, A. Hughes, and P. Clarkson, "Improved load modelling for emerging distribution system assessments," *CIRED Open Access Proceedings Journal*, vol. 2021, no. 1, pp. 1301–1305, 2021.
4. D. Del Giudice, F. Viola, and M. Rinaldi, "Definition of static and dynamic load models for grid studies of electric vehicles connected to fast charging stations," *arXiv preprint* arXiv:2302.03943, 2023.
5. D. Madjovski, I. Dumancic, and L. Petkovska, "Dynamic modeling of distribution power systems with renewable generation for stability analysis," *Energies*, vol. 17, no. 20, p. 5178, Oct. 2024.
6. Bokhari, R. Billinton, and W. Xu, "Experimental determination of the ZIP coefficients for modern residential, commercial, and industrial loads," *IEEE Trans. Power Delivery*, vol. 29, no. 3, pp. 1447–1455, Jun. 2014.
7. J. Li, H. Zhao, and Y. Wei, "A practical short-circuit current calculation method for renewable energy plants based on single-machine multiplication," *Electricity*, vol. 6, no. 1, p. 7, 2025.
8. Niersbach, A. Ghourabi, and A. Hanson, "Advanced modelling of inverter-based generators for short-circuit current calculations based on IEC 60909-0:2016," in *Proc. CIRED Conf.*, 2019.
9. M. S. Nizam, R. Islam, and M. T. Rahman, "Comparison of peak short-circuit current between traditional and renewable energy sources," in *Proc. IET Conf. on Renewable Power Generation*, 2023.
10. T. Riedlinger, P. Wintzek, and M. Zdrallek, "Development of a new modelling concept for power flow calculations across voltage levels," *Electricity*, vol. 5, no. 2, p. 10, 2024.
11. O. D. Montoya, A. Rajagopalan, and F. Moya, "Optimal capacitor placement and its effect on distribution network operation," *Mathematics*, vol. 10, no. 16, p. 1600, 2022.
12. H. Jayasinghe, K. Gunawardane, and R. Nicholson, "Applications of electrical load modelling in digital twins of power systems," *Energies*, vol. 18, no. 4, p. 775, Feb. 2025.
13. T. Huang, L. Li, and K. Zhang, "Optimal operation of renewable energy bases considering short-circuit ratio and transient overvoltage constraints," *Energies*, vol. 18, no. 5, p. 1256, Mar. 2025.
14. R. Zhang, K. Qu, and C. Zhao, "Robust distribution network reconfiguration using mapping-based column-and-constraint generation," *arXiv preprint* arXiv:2505.24677, 2025.
15. Abdelaziz, A. El-Dib, and R. El-Shatshat, "Distribution load flow methods for modern distribution systems: A review," *Electric Power Systems Research*, vol. 163, pp. 616–627, Oct. 2018.
16. H. Saadat and D. Manz, "Newton-Raphson power flow for distribution systems with distributed generation," *Int. J. of Electrical Power & Energy Systems*, vol. 78, pp. 802–813, 2016.
17. Y. Sun, J. Zhang, and L. Wang, "Probabilistic load flow calculation of AC/DC hybrid system based on cumulant method," *arXiv preprint* arXiv:2201.12571, 2022.
18. M. Yang, R. Xie, and Y. Zhang, "Robust microgrid dispatch with real-time energy sharing and endogenous uncertainty," *arXiv preprint* arXiv:2403.15219, 2024.
19. L. Yang, H. Yang, and X. Cao, "Distributionally robust frequency-constrained microgrid scheduling towards seamless islanding," *arXiv preprint* arXiv:2401.03381, 2024.
20. K. Hoseinzadeh and F. Blaabjerg, "A novel control technique for on-load tap changer to enlarge reactive power capability of wind power plants," *IET Generation, Transmission & Distribution*, vol. 16, pp. 2928–2938, 2022.

21. K. Yoon, J. Shin, and T. Nam, "Operation method of on-load tap changer on main transformer considering reverse power flow in distribution system connected with high penetration of photovoltaic system," *Energies*, vol. 15, no. 17, p. 6473, 2022.
22. H. Luo, J. Wu, and Z. Wang, "A dynamic reconfiguration model and method for load balancing in the snow-shaped distribution network," *Frontiers in Energy Research*, vol. 12, p. 1361559, 2024.
23. E. Zarate-Perez, J. Silva, and F. Lopez, "Assessment and optimization of residential microgrid based on PV, wind & BESS using GA and ACO," *Processes*, vol. 13, no. 3, p. 740, 2025.
24. S. Phommixay, M. Doumbia, and D. Lupien St-Pierre, "Review on the cost optimization of microgrids via particle swarm optimization," *Energy Systems*, vol. 11, pp. 445–468, 2020.
25. ETAP, *ETAP Power System Analysis User Guide – Load Flow and Short-Circuit Modules*, Operation Technology Inc., 2020.